Automatic Detection of the Anterior and Posterior Commissures on MRI Scans using Regression Forests

Yuan Liu, *IEEE Student Member*, and Benoit M. Dawant, *IEEE Fellow*

Abstract— **Identification of the anterior and posterior commissure is crucial in stereotactic and functional neurosurgery, human brain mapping, and medical image processing. We present a learning-based algorithm to automatically and rapidly localize these landmarks using random forests regression. Given a point in the image, we extract a set of multi-scale long-range textural features, and associate a probability for this point to be the landmark. We build random forests models to learn the relationship between the value of these features and the probability of a point to be a landmark point. Three-stage coarse-to-fine models are trained for AC and PC separately using down-sampled by 4, down-sampled by 2, and the original images. Testing is performed in a hierarchical approach to first obtain a rough estimation at the coarse level and then fine-tune the landmark position. We extensively evaluate our method in a leave-one-out fashion using a large dataset of 100 T1-weighted images. We also compare our method to the state-of-art AC/PC detection methods including an atlas-based approach with six well-established nonrigid registration algorithms and a publicly available implementation of a model-based approach. Our method results in an overall error of 0.84±0.41mm for AC, 0.83±0.36mm for PC and a maximum error of 2.04mm; it performs significantly better than the model-based AC/PC detection method we compare it to and better than three of the nonrigid registration methods. It is much faster than nonrigid registration methods.**

I. Introduction

The anterior commissure (AC) and posterior commissure (PC) are white matter fibers bundles that connect two cerebral hemispheres of the brain. AC and PC are important brain structures and crucial landmarks for stereotactic and functional neurosurgery, human brain mapping, and medical image processing [1]-[3]. For example, in deep brain stimulation (DBS) procedures, target locations could be determined by their relative position to the origin of a standardized coordinate system defined by AC, PC and the mid-sagittal plane [1]. Major stereotactic brain atlases, such as the Talairach and Tournoux atlas [4] and the Schaltenbrand-Wahren atlas [5], rely on AC and PC to establish the standard alignment of the brain. AC and PC could also be used to estimate an initial affine transformation between two volumes prior to any nonrigid registration [6].

This research is supported by NIH grant R01-EB006136 from the National Institute of Biomedical Imaging and Bioengineering.

Yuan Liu is with the Department of Electrical Engineering and Computer Science, Vanderbilt University, Nashville, TN 37205 USA (phone: 615-496-8059; e-mail: yuan.liu@vanderbilt.edu).

Benoit M. Dawant is with the Department of Electrical Engineering and Computer Science, Vanderbilt University, Nashville, TN 37205 USA (e-mail: benoit.dawant@vanderbilt.edu).

In most current neuroimaging applications, AC and PC are selected manually on the MRI scans by the experts. However, this requires expertise and suffers from inter-expert variability, which can have a substantial effect on targeting in image guided neurosurgery [7]. Manual intervention also takes time and prevents the automated use of information about the AC/PC position by other image processing techniques such as registration. Over the years, several approaches have been proposed to automatically localize AC and PC on 3D MRI scans [6], [8]-[13]. All of these algorithms rely on successful segmentation of surrounding structures, localization of other anatomical landmarks, or image registrations. For example, in [6], [8]-[10], the corpus callosum was used to initialize the AC and PC positions. Ardekani *et al.* achieved the initialization by identifying the mid-sagittal plane and a landmark on the midbrain-pons junctions [11]. Han *et al.* and Verard *et al.* also relied on edge detection [6], [8]. In [12], [13], atlas-based nonrigid registration was performed to transfer the AC and PC positions from atlases onto subjects. However, segmentations of surrounding structures, landmark detection, edge detection, and nonrigid registration algorithms may fail because of large anatomical variations or image contamination such as noise or partial volume effect, leading to the failure of AC/PC detection. In addition, some of these methods require adjusting a large set of parameters and long runtimes, especially for registration based methods.

Recently, learning-based methods using random forests have gained popularity for landmark detection. Random forests are an ensemble supervised learning technique for classification or regression. It constructs a multitude of decision trees by evaluating a random subset of features at each node to split the data and aggregates the output of each tree as final prediction [14]. In [15], Dabbah *et al.* used random forests as a classifier to localize anatomical landmarks in CT. Hough forests, which combines random forests with generalized Hough transform, are applied to detect points of a point distribution model on 2D radiographs [16], and rough positions for centers of vertebrae in MR images [17]. Here, we investigate its application to AC/PC localization. Since AC and PC have different local appearances from other points, we hypothesize that a nonlinear regression can be used to estimate the relationship between the local appearance of a point and its probability to be the AC/PC.

The algorithm we propose is fast, accurate, and robust. It also does not rely on any preprocessing of the images such as edge enhancement, nor does it require any segmentation or registration. Instead, we extract multi-scale textural features for points in the training images and build random forests regression models to learn the probability for each sample to be the AC/PC. We employ three-stage coarse-to-fine models, with the first one searching on a down-sampled image to

roughly localize the landmark and the second and third models to fine-tune the landmark position. We evaluate our algorithm extensively in a leave-one-out fashion using a large dataset of 100 subjects. We also compare our method to the state-of-art AC/PC detection methods including an atlas-based approach with six well-established nonrigid registration algorithms and a publicly available implementation of a model-based approach.

II. Methods

A. Image Data

We select 100 subjects from the data repository we have created over a decade for DBS surgeries. All images in our data set are T1-weighted sagittal MR image volumes with approximately 256×256×170 voxels and 1 mm in each direction, acquired with the SENSE parallel imaging technique (T1 W/3D/TFE) on a 3 Tesla Phillips scanner (TR = 7.92 ms, TE = 3.65 ms). These images have similar pose with small differences in head orientation and position. They also have similar field of view (FOV), i.e., they cover the entire head. All images have been acquired as part of the normal delivery of care and every subject was consented to participate in this study.

For each subject, AC and PC points were manually identified by two raters. These two raters followed the same protocol to select AC/PC and were given sufficient time for accurate localization. The inter-rater variability is 0.57±0.47mm for AC and 0.57±0.37mm for PC. Gold standard AC/PC points are computed as the average of the selections by the two raters and used for training and testing in the following sections.

B. Problem Formulation

We use a voxel-level training solution based on regression forests for each landmark. For each voxel, we extract a set of features that describes contextual variation at different scales, as proposed by Pauly *et al.* [18]. This is realized by applying a random displacement to this voxel x, calculating the mean intensities of a 3D cuboidal region R_x^s centered on x and of a similar region $Q_x^{s,m}$ of the same size but centered on the displaced voxel, and subtracting these two:

$$f^m = \frac{1}{|R_x^s|}\left(\sum_{x' \in Q_x^{s,m}} I(x') - \sum_{x' \in R_x^s} I(x')\right) \quad (1)$$

where I is the intensity, and s is the current scale, i.e., the size of the cuboidal region. Four scales are used and they correspond to window sizes of 4, 8, 16, and 32. This process is repeated $M = 2000$ times to obtain the feature set $\{f^m\}_{m=1}^M$.

Each voxel is associated with a probability p to be the landmark that the model is trained to detect. This probability follows a truncated Gaussian distribution according to its Euclidean distance d to the gold standard of this landmark:

$$p = \begin{cases} \frac{1}{\sqrt{2\pi}\sigma} e^{-\frac{d^2}{2\sigma^2}} & p > 0.1 \\ 0 & p \le 0.1 \end{cases} \quad (2)$$

where $\sigma = 3$ is the standard deviation. We truncate the probability function to speed up the training process.

Given a number of training pairs $\{\vec{f}_n, p_n\}_{n=1}^N$, the random forests aims to learn a nonlinear mapping from the feature space $\{\vec{f}\}$ to the probability space $\{p\}$. Hence the landmark detection problem can now be formulated as finding the voxel associated with the highest probability. This voxel indicates the most likely position of the AC/PC.

C. Regression Forests

We use 20 regression trees to construct the forests. For each tree, a bootstrap of two thirds of training samples is randomly selected and fed to the root node of the tree. Given the training samples $\{\vec{f_n}, p_n\}_{n=1}^{N'}$ at a particular node, we seek to select a feature f^m and a threshold t to best split the data. The splitting criterion minimizes:

$$MSE_T(t) = MSE(\{p_n : f_n^m < t\}) + MSE(\{p_n : f_n^m \ge t\}) \quad (3)$$

where MSE is the mean squared error. A subset of 500 features is randomly selected to examine the splitting threshold. The tree stops growing if the number of samples arriving at leaf nodes is smaller than 5 or if the best split threshold cannot be found.

Each leaf of the regression trees stores the mean p of all samples arriving at that node and this is used as predictor. When a test sample comes, each tree contributes to a prediction and the final prediction is made by averaging the outputs of all trees.

D. Training Phase

We build three stage coarse-to-fine models for AC and PC separately, one on down-sampled by 4 images, one on down-sampled by 2 images, and one on full resolution images. Since all images in our dataset have similar pose and FOV, landmarks could be localized in a region of interest instead of searching through the entire image. Hence when training the model, for each image, we only evaluate a set of points on a grid within a region of interest centered on the gold standard AC/PC. Empirically we choose the size of this region to be a 15×15×15 voxel^3 cube for each resolution level. This covers up to a 60×60×60 mm^3 area at the coarsest level, and we have found it large enough to localize the landmark with the variation in AC/PC positions we have observed across all images in the dataset.

E. Testing Phase

Given a test image, following the hierarchical approach, we first down-sample the image by 4 and start testing using the model built at this resolution level. We initialize the search center for this model by averaging the gold standard landmark positions of all training subjects, and search within a 21×21×21 window on a regular grid. A response map is generated, displaying the probabilities of the voxels to be the trained landmark. The voxel associated with the highest probability is then used as the search center for the next resolution. The final landmark position is the voxel location with the highest probability at the full resolution level.

F. Comparison to Other Methods

We compare our results with those obtained by atlas-based registrations, including affine only, and affine + nonrigid registrations, a technique routinely used for automatic identification in DBS procedures [12]. We choose one atlas

used by Pallavaram *et al.* [12] to be the reference and project its AC and PC points onto the 100 subjects through registration. An affine transformation is estimated first using intensity-based technique. The results obtained after this step are visually checked and corrected, if necessary. Then nonrigid registration is performed with a series of well-established algorithms, including the Adaptive Basis Algorithm (ABA) [19], the Adaptive Basis Algorithm with bounding box (LABA) [19], Diffeomorphic Demons (DD) [20], Symmetric Normalization (SyN) [21], Fast Free Form Deformation (F3D) [22], and Automatic Registration Toolbox (ART) [23]. A detailed description of those algorithms can be found in [24]. We also compare our method to a model-based method that has been recently proposed and we refer to it as MD (Model-based Detection). To do so, we use a publicly available implementation of this technique [11].

III. Results

We have conducted a leave-one-out validation, which uses 99 volumes for training and the last one for testing, and repeats this process 100 times.

A qualitative example of the response maps for AC in one test image at the full resolution level is shown in Fig. 1, with the map overlaid on top of the original image and the cross indicating the gold standard AC point. As shown in Fig. 1, this gold standard point has a high probability and is very close to the peak of the map (0.48 mm).

To quantitatively evaluate the accuracy of the algorithm, we use the 3D Euclidean distance between the automatically detected landmarks and the gold standard as a measure of error. We refer to our algorithm as RF (Random Forests) in the following text. Fig. 2 shows the box plot of errors using different methods for AC and Fig. 3 for PC. There are some outliers with errors beyond the maximum range of the y axis (12 mm), thus not shown in these figures. This includes 2 cases using Affine, 4 cases using MD for AC, and 4 cases using MD for PC. We also report error statistics for AC in Table I and PC in Table II. We have excluded those above-mentioned outliers with errors larger than 12 mm for Affine and MD when computing their mean, maximum, and standard deviations in order not to bias the comparisons. Table I and II demonstrate that our method leads to smaller mean, maximum, and standard deviation of errors for AC and PC compared to registration-based results including Affine, ABA,

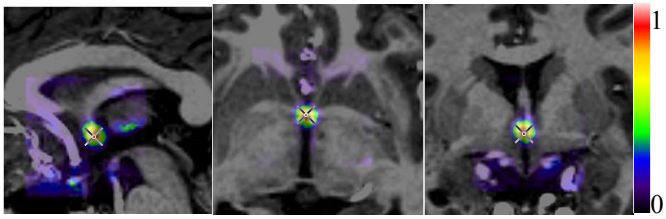

Figure 1. Example of the response map for AC.

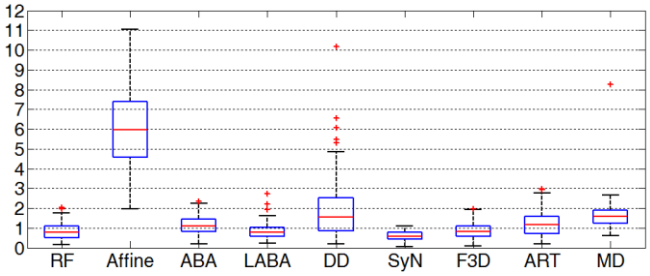

Figure 2. Boxplot of errors for AC.

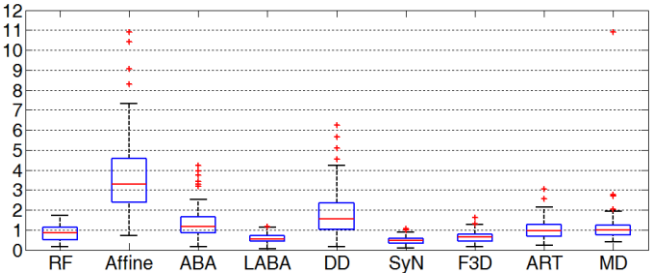

Figure 3. Boxplot of errors for PC.

TABLE I. STATISTICS OF ERRORS BETWEEN THE AC DETECTED AUTOMATICALLY USING DIFFERENT METHODS AND THE GOLD STANDARD AC POSITIONS

Error (ε): (mm) (AC)	Cases with ε <1	Cases with 1≤ ε <2	Cases with 2≤ ε <3	Cases with ε ≥3	Mean	Max.	Std.
RF	67	31	2	0	0.84	2.04	0.41
Affine	0	1	2	97	5.96	11.06	1.87
ABA	43	53	4	0	1.12	2.35	0.48
LABA	73	25	2	0	0.83	2.73	0.40
DD	29	32	22	17	1.96	10.18	1.58
SyN	94	6	0	0	0.60	1.10	0.24
F3D	67	33	0	0	0.86	1.98	0.39
ART	40	52	8	0	1.19	2.99	0.60
MD	17	65	13	5	1.58	8.26	0.82

TABLE II. STATISTICS OF ERRORS BETWEEN THE PC DETECTED AUTOMATICALLY USING DIFFERENT METHODS AND THE GOLD STANDARD PC POSITIONS

Error (ε): (mm) (PC)	Cases with ε <1	Cases with 1≤ ε <2	Cases with 2≤ ε <3	Cases with ε ≥3	Mean	Max.	Std.
RF	60	40	0	0	0.83	1.71	0.36
Affine	1	13	28	58	3.68	10.90	1.88
ABA	38	51	5	6	1.33	4.23	0.75
LABA	93	7	0	0	0.57	1.18	0.23
DD	23	43	22	12	1.83	6.25	1.15
SyN	99	1	0	0	0.47	1.07	0.19
F3D	90	10	0	0	0.66	1.61	0.28
ART	54	43	2	1	1.02	3.04	0.49
MD	51	41	3	5	1.13	10.91	1.09

TABLE III. *P* VALUES OF WILCOXON TESTS BETWEEN THE ERRORS OF AC/PC DETECTED BY OUR METHOD AND ERRORS OF THOSE DETECTED BY OTHER AUTOMATIC METHODS

P	Affine	ABA	LABA	DD	SyN	F3D	ART	MD
AC	**0.00**	**0.00**	0.65	**0.00**	1.00	0.32	**0.00**	**0.00**
PC	**0.00**	**0.00**	1.00	**0.00**	1.00	1.00	**0.01**	**0.00**

DD, and ART, as well as the AC/PC detection method MD.

In addition, we perform one-sided paired Wilcoxon signed-rank statistical test to test whether or not our method leads to errors that are smaller than those obtained with the other techniques. The *p* values are shown in Table III. *P* values smaller than the significance level of 0.05 are marked in red bold, suggesting that the errors of our method is statistically significantly smaller than that of the other method. As shown in Table III, our method significantly reduces the AC/PC localization errors compared to the registration-based approaches using Affine, ABA, DD and ART. It also outperforms the AC/PC detection method MD.

All computations are done on the Advanced Center for Computing and Research Education (ACCRE) Linux cluster at Vanderbilt University. The approximate CPU runtime for our algorithm is 8 seconds on a standard PC using one CPU core and 4GB RAM, whereas it takes 4.5, 25, 9, 40, 97, 45, 30 minutes for Affine, ABA, LABA, DD, SyN, F3D, and ART respectively, and 25 seconds for MD.

IV. Discussion and Conclusion

In this paper, we propose a learning-based method to automatically detect AC and PC landmarks in MRI brain scans using random forests regression. Our approach does not require any pre-processing steps and does not rely on any segmentations or registrations. Results of the leave-one-out experiments have shown that our approach is accurate and robust, with 0.84±0.41mm errors for AC, 0.83±0.36mm errors for PC, and a maximum error of 2.04 mm.

We have also compared our approach to single atlas based methods using six well-established nonrigid registration algorithms and also with a model-based approach proposed recently. We have found that our algorithm outperforms three nonrigid registration methods (ABA, DD, and ART) as well as the AC/PC detection method MD in terms of accuracy and robustness; the improvements are statistically significant. Other registration methods (LABA, SyN, and F3D) achieve better accuracy than ours. However, they rely on good affine initialization. In this study we have manually corrected 9 out of the 100 affine registrations so as not to bias the nonrigid registration results. However, in an automatic system such inaccurate affine registration may deteriorate the performance of nonrigid registrations and cause a failure in ACPC detection.

Another advantage of our approach is the speed. Although registration methods such as SyN may be more accurate, they generally take substantially longer than our algorithm. The algorithm is implemented in C++ with Matlab interfaces, and could potentially be speeded up with parallelization. Our method is also extendable to other image modalities by building models for that particular image set. Future work will include detection of AC/PC in other modalities.

References

[1] P. A. Starr, "Placement of deep brain stimulators into the subthalamic nucleus or globus pallidus internus: technical approach," *Stereotact. Funct. Neurosurg.*, vol. 79, no. 3-4, pp. 118-145, Jul. 2003.

[2] W. L. Nowinski, and A. Thirunavuukarasuu, "Atlas-assisted localization analysis of functional images," *Med. Imag. Anal.*, vol. 5, no. 3, pp. 207-220, Sep. 2001.

[3] D. L. Collins et al., "Automatic 3D intersubject registration of MR volumetric data in standardized Talairach space," *J. Comput. Assist. Tomo.*, vol. 18, no. 2, pp. 192-205, Mar./Apr. 1994.

[4] J. Talairach and P. Tournoux, *Co-planar Stereotaxic Atlas of the Human Brain*. New York: Thieme, 1988.

[5] G. Shaltenbrand, and W. Wahren, *Guide to the Atlas for Stereotaxy of the Human Brain*. Stuttgart, Germany: Thieme, 1977.

[6] Y. Han, and H. Park, "Automatic brain MR image registration based on Talairach reference system," in *Proc. IEEE Int. Conf. on Image Processing*, 2003, pp. 1097-1100.

[7] S. Pallavaram et al., "Intersurgeon variability in the selection of anterior and posterior commissures and its potential effects on target localization," *Stereotact. Funct. Neurosurg.*, vol. 86, no. 2, pp. 113-119, Mar. 2008.

[8] L. Verard et al., "Fully automatic identification of AC and PC landmarks on brain MRI using scene analysis," *IEEE Trans. on Med. Imag.*, vol. 16, no. 5, pp. 610-616, Oct. 1997.

[9] K. N. Bhanu Prakash, Q. Hu, A. Aziz, and W. L. Nowinski, "Rapid and automatic localization of the anterior and posterior commissure point landmarks in MR volumetric neuroimages," *Academic radiology*, vol. 13, no. 1, pp. 36-54, Jan. 2006.

[10] G. Zhang et al., "Automatic localization of AC and PC landmarks in T2-weighted MR volumetric neuroimages," in *Proc. IEEE Int. Conf. on Information and Automation*, 2010, pp. 1830-1834.

[11] B. A. Ardekani, and A. H. Bachman, "Model-based automatic detection of the anterior and posterior commissures on MRI scans," *NeuroImage*, vol. 46, no. 3, pp. 677-682, Jul. 2009.

[12] S. Pallavaram et al., "Validation of a fully automatic method for the routine selection of the anterior and posterior commissures in magnetic resonance images," *Stereotact. Funct. Neurosurg.*, vol. 87, no. 3, pp. 148-154, Jun. 2009.

[13] P. Anbazhagan, A. Carass, P. L. Bazin, and J. L. Prince, "Automatic estimation of midsagittal plane and AC-PC alignment on nonrigid registration," in *Proc. IEEE Int. Sym. on Biomed. Imag.: Nano to Macro*, 2006, pp. 828-831.

[14] L. Breiman, "Random forests," *Machine learning*, vol. 45, no. 1, pp. 5-32, Oct. 2001.

[15] M. A. Dabbah et al., "Detection and location of 127 anatomical landmarks in diverse CT datasets," in *Proc. SPIE Med. Imag.*, 2014, pp. 903415-903415.

[16] C. Lindner, S. Thiagarajah, J. M. Wikinson, J. C. Loughlin, G. A. Wallis, and T. F. Cootes, "Fully Automatic Segmentation of the Proximal Femur Using Random Forest Regression Voting," *IEEE Trans. on Med. Imag.*, vol. 32, no. 8, pp. 181-189, Aug. 2013.

[17] B. Glocker, J. Feulner, A. Criminisi, D. R. Haynor, and E. Konukoglu, "Automatic localization and identification of vertebrae in arbitrary field-of-view CT scans," in *Proc. Med. Image Comput. Comput.-Assisted Intervention Conf.*, 2012, pp. 590-598.

[18] O. Pauly et al., "Fast multiple organ detection and localization in whole-body MR Dixon sequences," in *Proc. Med. Image Comput. Comput.-Assisted Intervention Conf.*, 2011, pp. 239-247.

[19] G. K. Rohde, A. Aldroubi, and B. M. Dawant, "The adaptive bases algorithm for intensity-based nonrigid image registration," *IEEE Trans. on Med. Imag.*, vol. 22, no. 11, pp. 1470-1479, Nov. 2003.

[20] T. Vercauteren, X. Pennec, A. Perchant, and N. Ayache, "Diffeomorphic demons: efficient non-parametric image registration," *NeuroImage*, vol. 45, no. 1, pp. S61-S72, Mar. 2009.

[21] B. B. Avants, C. L. Epstein, M. Grossman, and J. C. Gee, "Symmetric diffeomorphic image registration with cross-correlation: evaluating automated labeling of elderly and neurodegenerative brain," *Med. Imag. Anal.*, vol. 12, no. 1, pp. 26-41, Feb. 2008.

[22] M. Modat et al., "Fast free-form deformation using graphics processing units," *Comput. Meth. Prog. Bio.*, vol. 98, no. 3, pp. 278-284, Jun. 2010.

[23] B. A. Ardekani et al., "Quantitative comparison of algorithms for inter-subject registration of 3D volumetric brain MRI scans," *J. Neurosci. Meth.*, vol. 142, no. 1, pp. 67-76, Mar. 2005.

[24] Y. Liu, P. F. D'Haese, and B. M. Dawant, "Effects of deformable registration algorithms on the creation of statistical maps for preoperative targeting in deep brain stimulation procedures," in *Proc. SPIE Med. Imag.*, 2014, pp. 90362B-90362B.